Chin. J. Astron. Astrophys. Vol. 6 (2006), No. 3, 312–322
(*http://www.chjaa.org*)

Chinese Journal of
Astronomy and
Astrophysics

Relative Spectral Lag: a New Redshift Indicator of Gamma-ray Bursts *

Zhi-Bin Zhang[1,4], Jia-Gan Deng[1,2], Rui-Jing Lu[1,2,4] and Hai-Feng Gao[3]

[1] National Astronomical Observatories/Yunnan Observatory, Chinese Academy of Sciences, Kunming 650011; *zbzhang@ynao.ac.cn*
[2] Physics Department, Guangxi University, Nanning 530004
[3] Sishui, No. 2 Middle School, Shandong 273206
[4] Graduate School of Chinese Academy of Sciences, Beijing 100049

Received 2005 October 28; accepted 2006 March 8

Abstract Using 64 ms count data of long gamma-ray bursts ($T_{90} > 2.6$ s), we analyze the quantity named relative spectral lag (RSL), $\tau_{31}/\mathrm{FWHM}_{(1)}$. We investigated in detail all the correlations between the RSL and other parameters for a sample of nine long bursts, using the general cross-correlation technique that includes the lag between two different energy bands. We conclude that the distribution of RSLs is normal and has a mean value of 0.1; that the RSLs are weakly correlated with the FWHM, the asymmetry, peak flux (F_p), peak energy (E_p) and spectral indexes (α and β), while they are uncorrelated with τ_{31}, the hardness-ratio (HR_{31}) and the peak time (t_m). Our important discovery is that redshift (z) and peak luminosity (L_p) are strongly correlated with the RSL, which can be measured easily and directly, making the RSL a good redshift and peak luminosity indicator.

Key words: gamma-rays: bursts — methods: data analysis

1 INTRODUCTION

The temporal profiles of gamma-ray bursts (GRBs) generally exhibit very complex and variable characteristics due to the overlapping between adjacent pulses (Norris et al. 1996; Quilligan et al. 2002). So far many investigations on the analysis of the light-curves especially the pulses have been made. For example, pulse properties, such as widths, amplitudes, areas and time intervals in between, together with number of pulses per burst, have been studied by several authors (e.g., McBreen et al. 1994, 2001, 2003; Li et al. 1996; Hurley et al. 1998; Nakar & Piran 2002; Qin et al. 2005).

In addition, some investigations involving the spectra have also been made (e.g., Kouveliotou et al. 1993; Hurley et al. 1992; Ghirlanda et al. 2004a). In particular, the spectral lag between the variation signals in different energy bands not only reflects the spectrum's evolution but also exhibits the properties of the light-curve. Researches on this feature have been done by various authors from many distinct aspects (see, e.g., Norris et al. 2000, 2001, 2005; Gupta et al. 2002; Kocevski & Liang 2003; Daigne & Mochkovitch 2003; Schaefer 2004; Li et al. 2004; Chen et al. 2005). Interestingly, it is found that, unlike short GRBs the spectral lags of most long GRBs are non-zero and are concentrated on the short end of the lag distribution, near 100 ms (Band 1997; Norris et al. 2001).

∗ Supported by the National Natural Science Foundation of China.

Concerning redshift (or luminosity) indictors of GRBs, previous investigations have offered some significant paradigms in the light-curves, for instance, the luminosity-lag relation (Norris et al. 2000) and the luminosity-variability relation (Reichart et al. 2001). A particular relation between the lag and the variability has been strongly confirmed to prove that both above luminosity indicators are reliable (Schaefer et al. 2001). Other indicators based on GRB spectral features have also since been constructed, based on either the $E_p - E_{\rm iso}$ relation (Amati et al. 2002; Atteia 2003), the $E_p - L_p$ relation (e.g., Yonetoku et al. 2004) or the $E_p - E_\gamma$ relation (Ghirlanda et al. 2004b). The spectra and the light-curves are related to each other, via the spectral lag.

Norris et al. (2004, 2005) found that a wide pulse width is strongly correlated with the spectral lag and these two parameters may be viewed as mutual surrogates when estimating the GRB luminosity and total energy. Motivated by the above-mentioned developments, our first aim is to analyze the RSLs (relative spectral lags) of long bursts to find out their number distribution. Further purpose of this work is to search for possible relations between the RSL and some other parameters, and then interpret them in physical terms. Our data preparation is presented in Section 2. In Section 3 we are going to measure some typical physical variables. Section 4 shows all the results obtained. We then apply the RSLs to the observed data and try to reveal their physical explanations in Section 5. We shall end with a discussion and conclusions in Section 6.

2 DATA ANALYSIS OF PULSES

2.1 Sample Selection

We use 64 ms count data selected from the current BATSE catalog for long bursts, to make up our "Sample 1" that includes 36 sources. Note that here we only select bursts with single pulses. The highly variable temporal structure observed in most bursts is deemed to be produced by internal shocked outflow, provided that the source emitting the relativistic flow is variable enough (e.g., Dermer & Mitman 1999; Katz 1994; Rees & Mészáros 1994; Piran, Shemi & Narayan 1993). In this case, the temporal structure generally reflects the activity of the "inner engine" that drives the bursts (Sari & Piran 1997). As a result of overlap, it is generally difficult to determine how many pulses a complex burst should comprise or to model the shape of these pulses (Norris et al. 1996; Lee et al. 2000). Fortunately, the observed peaks have almost one-to-one correlation with the activity of the emitting source, i.e., each pulse is legitimately assumed to be associated with a separate emission episode of one burst (Kobayashi et al. 1997; Kocevski et al. 2003). On the other hand, the spectral parameters of distinct pulses within a burst are different from each other, which allows us to believe that the spectral lags between these pulses will show large differences (Hakkila & Giblin 2004; Ryde et al. 2005). Therefore, we restrict our sample to be composed of relatively simple and bright bursts dominated by a single pulse event (rather than dim or multi-peak bursts) for which we could accurately calculate the spectral lags.

The selection is not done with an automated program (e.g., Scargle 1998; Norris et al. 2001; Liang et al. 2002; Quilligan et al. 2002), rather, by simple experienced visual inspection, which to a certain degree could reduce any biases either from denoising techniques or from the pulse identification algorithm itself (Ryde et al. 2003). Lee et al. (2000) has found the number of pulses in a burst is usually different for different energy bands. In principle, a brightness-independent analysis is required for the burst duration measurement (Bonnell et al. 1997), while the level of S/N should be reasonable and reliable. Based on these considerations, the criteria for our sample selection are taken as follows: T_{90} duration > 2.6 s; BATSE peak flux $(50 - 300\,{\rm keV}) > 1.5$ photons cm^{-2} s^{-1}; and peak count rate $(> 25\,{\rm keV}) > 14\,000$ counts s^{-1}. Next, we will process the data with background subtraction and denoising.

2.2 Background Subtraction and Denoising

In general, the first step in data preparation is to select an appropriate background for subtraction. To handle these data as a whole, an alternative mode of processing involving background subtraction along with denoising is presented here. For each source, we take the signal data which cover as much as possible the full range of the pulse in order to ensure that contributions of all signals to the lags are included. From

experience, data beyond this range are regarded as the background. However, for convenience, we here prefer disposing of the whole data involving pre- and post-pulse for separate processing.

Considering the duration and background level of long bursts, we first smooth them with the DB3 wavelet with the MATLAB software and then fit them with a pulse function plus a quadratic form, namely

$$F(t) = F_m \Big(\frac{t}{t_m}\Big)^r \Big[\frac{d}{d+r} + \frac{r}{d+r}\Big(\frac{t}{t_m}\Big)^{(r+1)}\Big]^{-\frac{r+d}{r+1}} + at^2 + bt + c\,, \tag{1}$$

where the first expression on the right is quite a flexible function (see eq. (22), Kocevski et al. 2003) to be applied to describe the pulse shape, and the quadratic term represents a background that spans the whole data. The parameter t_m is the time of maximum flux, F_m, of the pulse, and the quantities r and d are two indexes describing the rise and fall of the pulse profile. After the background is subtracted from the fitted data, we have the pure signal data that are not contaminated by the background or noise to a certain error level. These signal data are just what we need to use for the analysis of the spectra and light-curves.

We divide our analyses into two portions in order to achieve different goals of calculations for Sample 1. One portion is to pre-treat the light-curve data in channels 1 and 3 (i.e., 25–55 keV and 110–320 keV) and define the signal data in these two channels as Sample 2. Another is to combine the data from all four channels in order to study the characteristics of the "bolometric" light-curve profile, e.g., FWHM and asymmetry. To avoid confusion of definitions, the signal data over all four channels are called Sample 3.

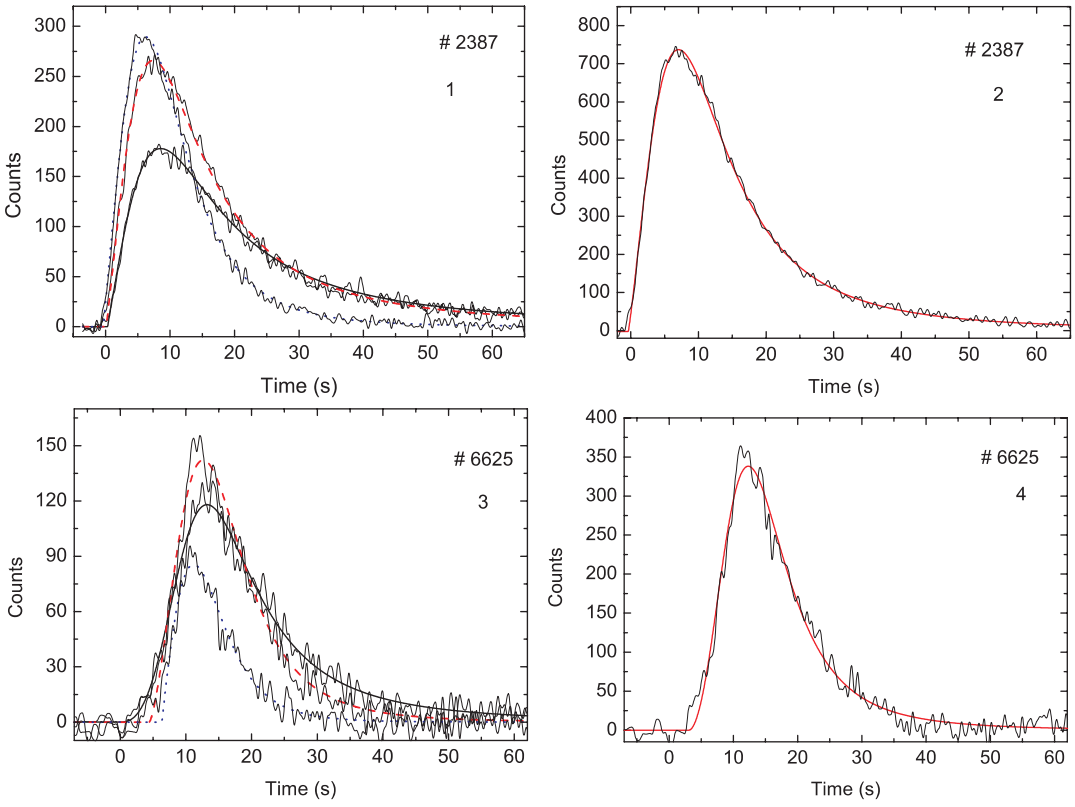

Fig. 1 Light-curves of two of the studied single-peaked events, one with good S/N (GRB 930612 #2387, panels 1 and 2), and one with poor S/N (GRB 980302 #6625, panels 3 and 4). Panels 1 and 3 display the best fit lines to the observed light-curves in channels 1 (25–55 keV, solid line), 2 (55–110 keV, dashed line) and 3 (110–320 keV, dotted line); and Panels 2 and 4, the best-fit "bolometric" light-curves resulting from all four channels.

Figure 1 displays two of the studied pulses (#2387 and #6625). Panels (1) and (3) show the best-fit curves to the profiles in channels 1, 2 and 3 and Panels (2) and (4), the best-fit to the "bolometric" profile resulting from all four channels.

3 MEASUREMENTS OF PHYSICAL QUANTITIES

In this section we focus our attention on the measurements of the quantities, RSL, FWHM and asymmetry of the single-peaked events in our sample of 36 long GRB pulses.

3.1 Relative Spectral Lag

For Sample 2 we calculated the cross-correlation function (CCF) (Band 1997) between channels j and k,

$$\mathrm{CCF}(\tau; \upsilon_j, \upsilon_k) = \frac{\langle \upsilon_j(t)\upsilon_k(t+\tau)\rangle}{\sigma_{\upsilon_j}\sigma_{\upsilon_k}}, \ \ (j \neq k) \tag{2}$$

where $\sigma_{\upsilon_i} = \langle \upsilon_i^2 \rangle^{1/2}$, i [=1, 2, 3 or 4] indicate the different channels; τ is the so-called spectral "lag" between channels j and k; υ_j and υ_k the two time series in the two channels. For our Sample 2, we have $j = 3$ and $k = 1$, and we write the lag as τ_{31}, differing from those previous definitions of spectral lag (e.g., Norris et al. 2000; Gupta et al. 2002). We otherwise define a quantity called RSL, namely

$$\tau_{\mathrm{rel},31} = \tau_{31}/\mathrm{FWHM}_{(1)}, \tag{3}$$

with $\mathrm{FWHM}_{(1)}$ being the full width at half maximum of the time profile of channel 1, τ_{31} is determined by the location of τ where the CCF peaks: at this point the CCF curve is nearly gaussian. If the data points close to peak are not dense enough, we shall interpolate them over a range including the peak. From its definition above, $\tau_{\mathrm{rel},31}$ is a dimensionless quantity.

3.2 FWHM & Asymmetry

For the light-curve of a source, its asymmetry and FWHM are fundamental shape parameters that should be determined first since they reflect the properties of the bursts. The key factor of this issue is that FWHM is associated with the energy of the photons detected by the observer (or the Lorentz factor with FWHM$\propto \Gamma^{-2}$ (see Qin et al. 2004)) and that the asymmetry is largely influenced by the co-moving pulse width when the burst duration is not too large, say, $T_{90} < 1000\,\mathrm{s}$ (Zhang & Qin 2005). Thus, the asymmetry and FWHM should provide us with clues to intrinsic burst parameters.

We now come to measure these parameters at a certain significance level (see Sect. 3.3). Note that unlike $\mathrm{FWHM}_{(1)}$ (in Eq. (3)) the FWHM here represents the full width at half maximum of the 'bolometric' light-curve profile. Asymmetry is defined by the ratio of the rise time (t_r) of FWHM of pulse to the decay time (t_d). With a simple algorithm, we easily calculate the above quantities. Sometimes when the data are sparse, we may need interpolation for a more precise calculation. Separate analysis was made on Samples 2 and 3.

3.3 Error Analysis

Equations (1)–(3) show that both the fitted and derived parameters will contain errors propagated directly or indirectly. It is necessary to ensure that the impact of the background on the observed variables has been eliminated from Equation (1) by the background subtraction. Assuming the error of observed time (t) is zero at any one of data points, we find that the error of flux should be caused by parameters F_m, t_m, r and d, i.e.,

$$\sigma(F) = \Big\{ \Big(\frac{\partial F}{\partial F_m}\Big)^2 \sigma^2(F_m) + \Big(\frac{\partial F}{\partial t_m}\Big)^2 \sigma^2(t_m) + \Big(\frac{\partial F}{\partial r}\Big)^2 \sigma^2(r) + \Big(\frac{\partial F}{\partial d}\Big)^2 \sigma^2(d) \Big\}^{1/2}. \tag{4}$$

In reverse, t can be expressed as $t \equiv t(x_1, x_2, x_3, x_4, x_5) = f^{-1}(F, F_m, t_m, r, d)$, so the error of t derived by the fit to the observed data should be

$$\sigma(t) = \Big\{ \sum_{i=1}^{5} \Big(\frac{\partial t}{\partial x_i}\Big)^2 \sigma^2(x_i) \Big\}^{1/2} = \Big\{ \sum_{i=1}^{5} \Big(\frac{\partial F}{\partial x_i} \Big/ \frac{\partial F}{\partial t}\Big)^2 \sigma^2(x_i) \Big\}^{1/2}. \tag{5}$$

Suppose the two ends of the FWHM are t_1 and t_2, then the errors of t_r, t_d and FWHM can be written as

$$\sigma(t_r) = [\sigma^2(t_1) + \sigma^2(t_m)]^{1/2}, \tag{6}$$

$$\sigma(t_d) = [\sigma^2(t_m) + \sigma^2(t_2)]^{1/2}, \tag{7}$$

$$\sigma(\mathrm{FWHM}) = [\sigma^2(\mathrm{t_1}) + \sigma^2(\mathrm{t_2})]^{1/2}, \tag{8}$$

where $t_r = t_m - t_1$, $t_d = t_2 - t_m$ and FWHM$= t_2 - t_1$. With the definition of asymmetry ($\equiv t_r/t_d$), its error can be gained by

$$\sigma(\mathrm{asymmetry}) = \mathrm{asymmetry} \times \Big[\Big(\frac{\sigma(\mathrm{t_r})}{\mathrm{t_r}}\Big)^2 + \Big(\frac{\sigma(\mathrm{t_d})}{\mathrm{t_d}}\Big)^2\Big]^{1/2}. \tag{9}$$

The term υ in Equation (2) actually represents the variable F in Equation (1) after background subtraction, which ensures that the error of CCF is caused by the fluxes fitted to channels 1 and 3, i.e.,

$$\sigma(\mathrm{CCF}) = \Big\{\Big(\frac{\partial \mathrm{CCF}}{\partial \upsilon_1}\Big)^2 \sigma^2(\upsilon_1) + \Big(\frac{\partial \mathrm{CCF}}{\partial \upsilon_3}\Big)^2 \sigma^2(\upsilon_3)\Big\}^{1/2}, \tag{10}$$

where $\sigma^2(\upsilon_1)$ and $\sigma^2(\upsilon_3)$ are respectively determined by Equation (4) in channels 1 and 3. In addition, Equation (2) can be in turn replaced by $\tau_{31} \equiv \tau_{31}(x_1, x_2, x_3) = f^{-1}(\mathrm{CCF}, \upsilon_1, \upsilon_3)$. Thus

$$\sigma(\tau_{31}) = \Big\{\sum_{i=1}^{3}\Big(\frac{\partial \tau_{31}}{\partial x_i}\Big)^2 \sigma^2(x_i)\Big\}^{1/2} = \Big\{\sum_{i=1}^{3}\Big(\frac{\partial \mathrm{CCF}}{\partial x_i}\Big/\frac{\partial \mathrm{CCF}}{\partial \tau_{31}}\Big)^2 \sigma^2(x_i)\Big\}^{1/2}. \tag{11}$$

It shows that the error of τ_{31} comes from not only these fitted parameters but also the $\sigma(\mathrm{CCF})$ itself. The errors of $\tau_{\mathrm{rel},31}$ can be deduced from Equations (2) and (3) by the following propagation relation, Equation (9):

$$\sigma(\tau_{\mathrm{rel},31}) = \tau_{\mathrm{rel},31} \times \Big[\Big(\frac{\sigma(\tau_{31})}{\tau_{31}}\Big)^2 + \Big(\frac{\sigma(\mathrm{FWHM}_{(1)})}{\mathrm{FWHM}_{(1)}}\Big)^2\Big]^{1/2}, \tag{12}$$

where parameters $\mathrm{FWHM}_{(1)}$ and $\sigma(\mathrm{FWHM}_{(1)})$ in channel 1 can be measured with the same way as what is used in Equation (8) as well as Equation (5).

In fact, for a given sample the rise time (t_r) and the decay time (t_d) have a linear correlation, $t_r \propto \zeta t_d$, with the coefficient ζ estimated to be 0.3–0.5 for most bursts (Norris et al. 1996). The exact value of ζ is uncertain because of the uncertainty in the burst parameters. For the same reason, the relation between τ_{31} and $\mathrm{FWHM}_{(1)}$, $\tau_{31} \approx 0.089\mathrm{FWHM}_{(1)}^{-0.42}$ (Norris et al. 2005), is also required to be calibrated with a larger sample. Otherwise, we cannot accurately determine the errors propagated from these connected parameters. So we assume they are independent. The errors caused by this assumption would be larger than otherwise, so we should point out that the assumption does not influence the credibility in our error analysis.

4 RESULTS

First we display the RSL distribution of long burst pulses (Sect. 4.1). To obtain its physical implications much of our investigation concentrates on one sub-sample, Sample 4, which includes nine GRBs of long-lag and wide-pulse with simpler physics owing to their more accurate measurements (Sect. 4.2).

4.1 The RSL Distribution

Taking $j = 3$, $k = 1$ and combining Equations (2) and (3), we derive the quantities τ_{31} and $\mathrm{FWHM}_{(1)}$ for Samples 2, then $\tau_{\mathrm{rel},31}$. The RSL distribution is displayed in Figure 2, from which we see that all the pulses have positive τ_{rel} in the range from 0 to 0.35, concentrating about the value 0.1.

Moreover, we fit the distribution with a gaussian function and obtained χ^2/dof=1.1 with $R^2 = 0.97$, which indicates that the observed distribution is consistent with the normal curve. However, the distributions of FWHM and spectral lags (or time intervals) are found to be lognormal instead of normal (see e.g., Mcbreen et al. 2003). In the following, we pay particular attention to the properties of $\tau_{\mathrm{rel},31}$, which will be studied in great detail.

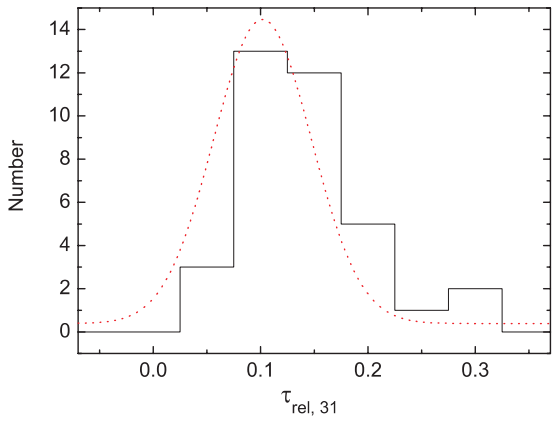

Fig. 2 Histogram of the distribution of RSLs for long bursts for a sample of 36 bright pulses. The smooth curve is the gaussian function fitted to the distribution, with mean value $\mu = 0.102$ and standard deviation $\sigma = 0.045$.

Table 1 Parameters fitted to Sample 4 with the model of this paper

Trigger	$\tau^{*}_{\rm rel,31}$	τ_{31} (s)	FWHM (s)	Asymmetry	$\rm HR_{31}$	F_m	t_m (s)
1406	0.126±0.017	1.47±0.15	9.64±0.30	0.43±0.03	0.85	464.09±2.19	4.47±0.05
2387	0.127±0.007	2.43±0.04	14.57±0.30	1.38±0.07	0.95	738.89±2.03	7.42±0.03
2665	0.166±0.014	1.47±0.10	4.56±3.40	0.44±0.51	0.45	327.94±2.49	3.22±0.26
3257	0.059±0.003	1.61±0.07	12.98±0.74	0.27±0.02	1.48	462.97±2.02	4.16±0.06
6504	0.105±0.006	2.02±0.06	9.78±1.13	0.36±0.07	1.49	457.78±3.15	4.39±0.11
6625	0.101±0.04	1.55±0.19	15.51±1.24	0.57±0.08	0.39	338.18±2.61	9.24±0.29
7293	0.092±0.009	1.84±0.06	12.11±2.66	0.31±0.09	1.74	626.78±2.76	5.32±0.15
7588	0.149±0.027	1.14±0.22	6.56±0.32	0.56±0.05	0.60	449.81±2.63	5.04±0.06
7648	0.192±0.036	2.19±0.30	11.94±0.60	0.55±0.05	2.12	305±4.02	6.89±0.13

Notes: symbol $*$ denotes the relative spectral lags calculated with Equations (2) and (3), as shown in Table 3.

4.2 Dependence of $\tau_{\rm rel,31}$ on the Light-curve Parameters

To investigate whether $\tau_{\rm rel,31}$ is associated with some parameters of the light-curve, we list the considered parameters in Table 1 and plot the relations in Figure 3. The hardness-ratio ($\rm HR_{31}$) here is defined as the ratio of photon counts of channel 3 to channel 1 in the pure signal data. The parameters F_m and t_m as well as their errors are taken from the fit with Equation (1).

To test these relations, we make a general linear correlation analysis (Press et al. 1992) and derive the correlation coefficients together with probabilities listed in Table 2. In Figure 3, the panels 'a', 'd' and 'f' show that, unless the data point (#7648) is removed, $\tau_{\rm rel,31}$ is evidently uncorrelated with τ_{31}, $\rm HR_{31}$ and t_m, despite a seeming trend of anti-correlation. The panels 'b', 'c' and e show that $\tau_{\rm rel,31}$ is positively correlated with the asymmetry, and negatively correlated with FWHM and F_m. It demonstrates that $\tau_{\rm rel,31}$ is very sensitive to the FWHM and the asymmetry, which suggests that it should be another parameter characterizing the shape of GRB pulses.

5 APPLICATIONS AND EXPLANATIONS

Encouraged by the special attributes of the $\tau_{\rm rel,31}$, we shall explore some other potential correlations, that will lead to physical interpretations.

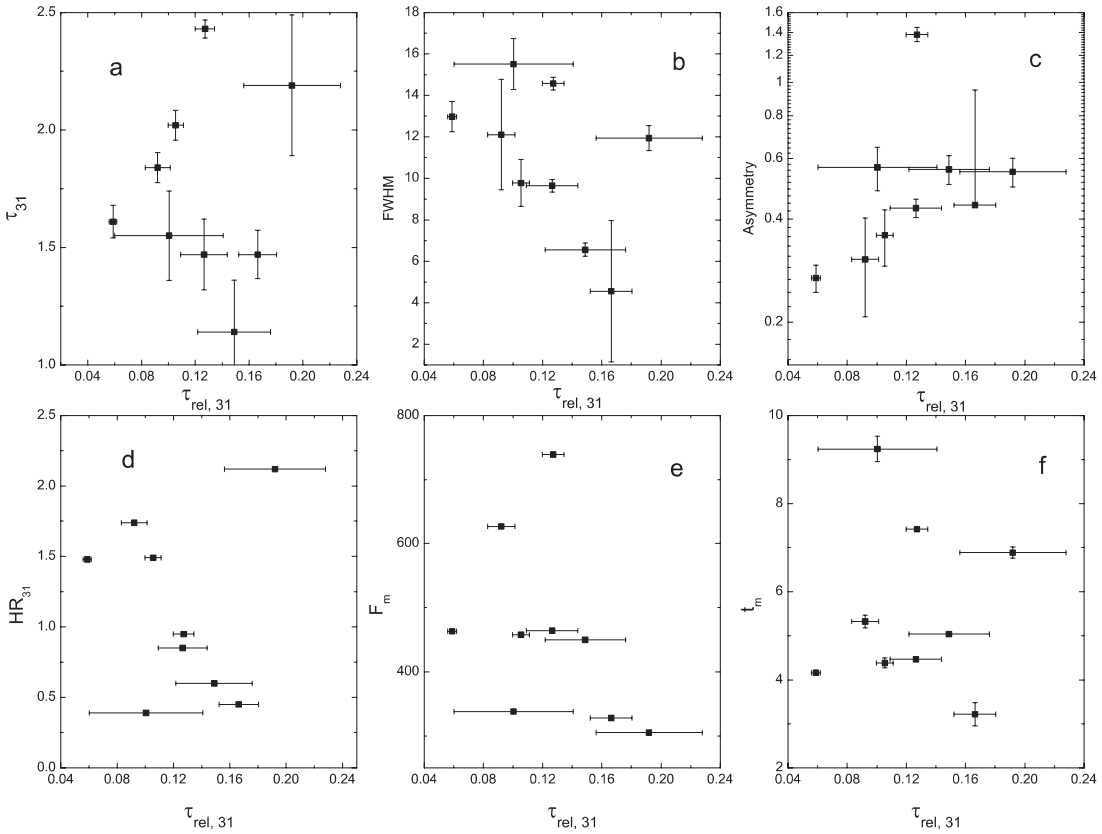

Fig. 3 Correlations between $\tau_{\rm rel,31}$ and the parameters of light-curves, τ_{31}, FWHM, asymmetry, $\rm HR_{31}$, F_m and t_m. These relations would be tighter if the source #7648 were excluded.

Table 2 Linear correlation analysis of Figures 3 and 4. Coefficient and probability are abbreviated to coef. and prob., respectively.

Panels		a	b	c	d	e	f
For Figure 3	coef.	0.08	–0.48	0.42	–0.04	–0.39	0.03
	prob.	0.84	0.19	0.25	0.92	0.29	0.95
For Figure 4	coef.	–0.40	0.32	–0.28	–0.89	–0.87	–0.51
	prob.	0.32	0.43	0.49	0.001	0.002	0.16

5.1 Detecting Relations between $\tau_{\rm rel,31}$ and other Physical Parameters

We first try to identify the appropriate variables for the present study. Since the determination of the energy spectrum as well as the distance (or energy) is usually the key issue in the understanding of the burst phenomenon, we opt to select the parameters α, β, E_p, z, L_p and F_p and seek their correlations with $\tau_{rel,31}$ (see Table 3).

We should point out that the redshifts of all the sources except #7648 were estimated from an empirical $E_p - L_p$ relation, rather than directly observed, because of the absence of information on the afterglow. The reason for selecting this $E_p - L_p$ relation is that it looks considerably tighter and more reliable than the relations given by the previous works (Yonetoku et al. 2004). The spectral parameters (α, β and E_p) for #2665 are unavailable at present.

Table 3 Parameters for the Observed and Modeled Data in Sample 4

Trigger (1)	$\tau^*_{\rm rel,31}$ (2)	$\alpha^{\rm a}$ (3)	$\beta^{\rm a}$ (4)	$E_p^{\rm a}$ (5)	$z^{\rm b}$ (6)	$L_p^{\rm b}$ (7)	$F_p^{\rm a}$ (8)
1406	0.126±0.017	–1.20±0.15	–2.89±0.21	79.43±21.39	1.91±0.4	22.8±10	2.13
2387	0.127±0.007	–0.03±0.09	–2.46±0.03	106.79±8.00	3.76±0.4	176±50	3.58
2665	0.166±0.014	——	——	——	1.19±0.11	11±2	1.91
3257	0.059±0.003	–0.24±0.09	–2.79±0.12	169.2±16.32	11.97±1.6	1750±600	2.62
6504	0.105±0.006	0.59±0.26	–2.78±0.17	120.2±20.34	1.67±0.07	40±4	2.25
6625	0.101±0.04	–1.18±0.12	–4.54±1.76	53.8±9.31	2.18±0.4	15.8±6	1.68
7293	0.092±0.009	–0.15±0.12	–2.81±0.11	151.1±17.41	8.48±3	733±500	2.73
7588	0.149±0.027	–1.73±0.38	–2.80±0.08	12.07±17.9	1.44±0.08	7.79±2.2	2.06
7648	0.192±0.036	–0.78±0.26	–2.43±0.21	146.93±58.0	0.43 [c]	0.54±0.1 [d]	1.53

Notes– Redshift (col. 6) and peak luminosity (col. 7) estimated by the $E_p - L_p$ relation were borrowed from Yonetoku et al. (2004) due to lack of information except trigger 7648 whose z and L_P (10^{51} erg s^{-1}) were given by Galama et al. (1999) and Guidorzi et al. (2005), respectively. Note the peak flux (F_p) is in units of photons cm^{-2} s^{-1}.
References.– a. Norris et al. (2005); b. Yonetoku et al. (2004); c. Galama et al. (1999); d. Guidorzi et al. (2005).

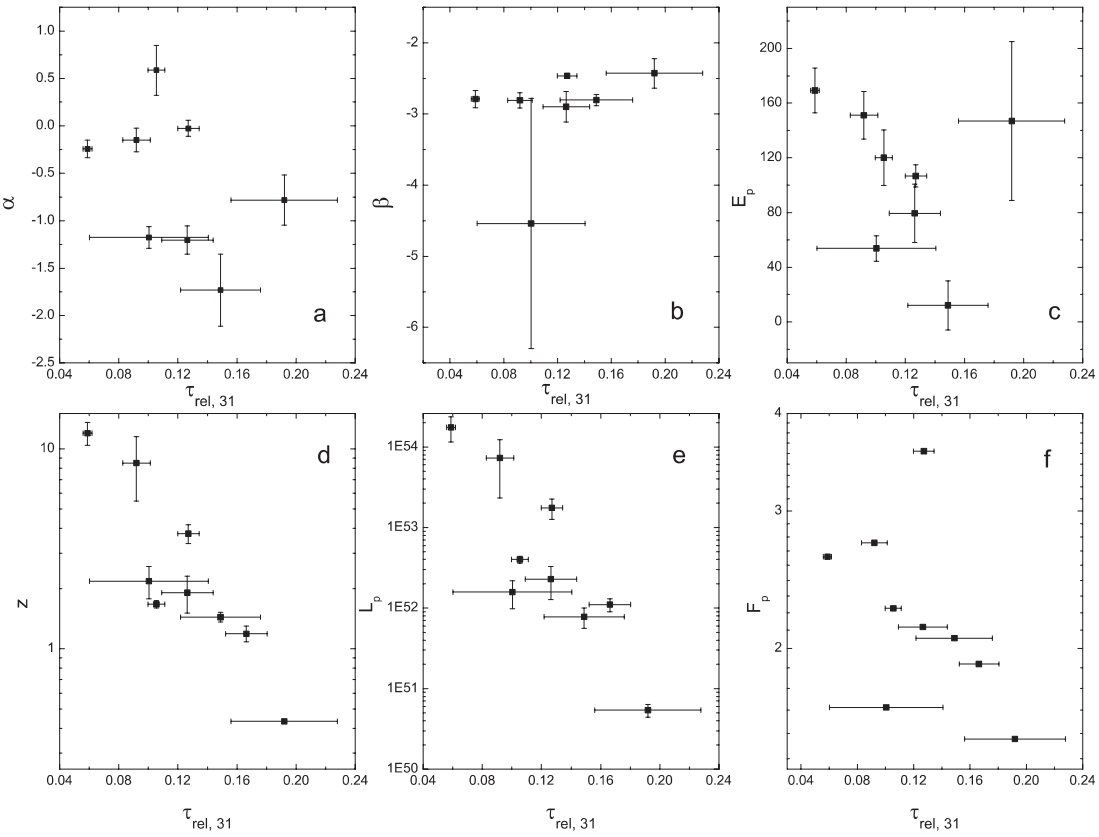

Fig. 4 Correlations between $\tau_{\rm rel,31}$ and the parameters α, β, E_p, z, L_p and F_p. The relations would again become tighter if the source #7648 were excluded.

All the correlations of $\tau_{\rm rel,31}$ with these parameters are shown in Figure 4. We apply the linear correlation analysis in the same way and the results are given in Table 2. Figure 4 shows that all the parameters except β are inversely correlated with $\tau_{\rm rel,31}$, while β, the high energy spectral index, shows a positive correlation with $\tau_{\rm rel,31}$. It has been pointed out that F_p is often used as an effective indictor of distance to the GRB source (Lee et al. 2000). The tight relation between $\tau_{\rm rel,31}$ and F_p in Figure 4f shows that $\tau_{\rm rel,31}$ is expected to be a distance indictor.

Surprisingly, we found from Figure 4d and 4e that $\tau_{\rm rel,31}$ is strongly correlated with z and L_p. Accordingly, our attempt in the next section is to confirm if $\tau_{\rm rel,31}$ is suitable as an indictor of distance or peak luminosity.

5.2 Redshift and Luminosity Indicator

As Atteia (2005) pointed out, whether a redshift indictor is good or not is determined by the degree of correlation between it and the redshift, i.e., by the size of the scatter in the correlation. The indicators are generally combinations of GRB parameters. To see whether or not $\tau_{\rm rel,31}$ is a good redshift indicator, we contrast the observed data with the theoretical model in Figure 5. Note that the data of Figure 5a and 5b are merely a replica of Figure 4d and 4e. From Figure 5a and 5b, the best fits to a linear model are

$$\log z \approx 1.56 - 9.66\tau_{\rm rel,31}, \tag{13}$$

$$\log L_p \approx 55.44 - 23.07\tau_{\rm rel,31}, \tag{14}$$

with spearman rank-order correlation coefficients of –0.88 ($p \sim 1.5 \times 10^{-3}$) for the former and –0.83 ($p \sim 5 \times 10^{-3}$) for the latter. This indicates the existence of a relatively accurate connection between the RSL and the redshift (or luminosity). Once $\tau_{\rm rel,31}$ is measured, we can use Equations (13) and (14) to obtain estimates of the redshift and peak luminosity without further information on the observed spectral lines. From this viewpoint, $\tau_{\rm rel,31}$ can be regarded as an ideal indicator of redshift and/or luminosity.

Meanwhile, RSLs might be utilized to constrain the cosmological parameters (say, Ω_m, Ω_λ and H_0) when the redshift and luminosity are determined by Equations (13) and (14) simultaneously. Certainly, the realization of this purpose requires us to eliminate in advance as much selection effects as possible, not only in the observations but also in the calculations.

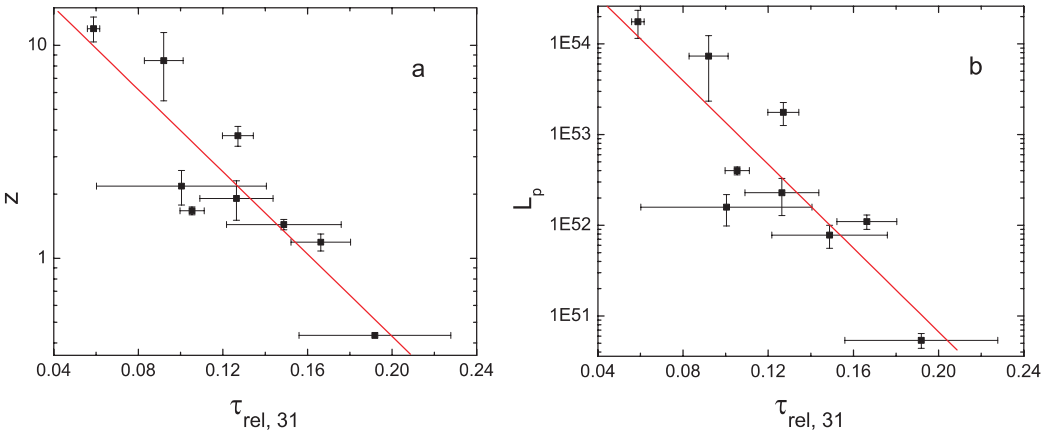

Fig. 5 Calibration curves for the relative spectral lag, $\tau_{\rm rel,31}$. Plots of $\tau_{\rm rel,31}$ vs. redshift and peak luminosity can be used to calibrate the redshift and/or luminosity indicator. The plots here can be fitted to yield Equations (13) and (14) (marked with the straight red lines in panels a and b).

6 CONCLUSIONS AND DISCUSSION

The above investigations lead the following conclusions: First, the RSL distribution is normal and is concentrated around the value 0.1. Secondly, the RSL is weakly correlated with the FWHM, asymmetry, α, β, E_p, F_p and F_m, and is uncorrelated with the lag_{31}, HR_{31} and t_m. Finally, we find $\tau_{\mathrm{rel},31}$ is a useful estimator of the redshift and peak luminosity.

In the internal shock model, GRBs generally consist of many pulses produced by multiple relativistic shells (or winds) followed by internal shocks due to collisions as the central engine pumps energy into the medium (e.g., Fenimore et al. 1993; Rees & Mészáros 1994). However, this does not conflict with our selecting only single peaked bursts in our sample. Furthermore, this manner of selection also avoids contamination by adjacent overlapping pulses which would inevitably produce additional errors. Under the assumption that these single wide pulses could be produced by the same mechanism (see Piran 1999), our motivation of this selection is advisable. In fact, McMahon et al. (2004) have pointed out that the favorite mechanism for producing such single pulse gamma-ray emission events may be external rather than internal shocks (see also Mészáros & Rees 1993; Sari & Piran 1996; Dermer et al. 1999, 2004).

It is usually expected that the gamma-rays come from a relativistically expanding fireball surface with Lorentz factor $\Gamma > 100$ (e.g., Lithwick et al. 2001). The bulk Lorentz factor increases linearly with the radius as long as the fireball is not baryon loaded and is not complicated by non-spherical expansion (Eichler et al. 2000) until $\Gamma > 1000$ (or $R \geq 10^{16}$ cm) (Woods et al. 1995). With the power density spectrum method, Spada et al. (2000) found the curvature time together with the dynamic time will dominate over the radiative cooling time at a distance $R < 5 \times 10^{14}$ cm. Given this, the FWHM has been found from the Doppler effect to follow FWHM$\propto \Gamma^{-2}$ (Qin et al. 2004). Assuming $\tau \propto \Gamma^{-\omega}$, we can deduce from Figure 3b that the upper limit of ω is about 2 which is compatible with $\tau \propto \Gamma^{-1}$ obtained by Shen et al. (2005).

In this work we have shown that the relative spectral lag can be used as an estimator of the redshift and peak luminosity of long GRBs. We note that our conclusion is based on an analysis of only nine sources. More accurate and robust results would require a larger sample of sources with redshifts. Up to now, no indicators have not been identified for short bursts, owing to lack of sufficient sources with redshift, in spite of the recent measurements and reports by Swift and HETE II (see, e.g., Bloom et al. 2005; Hjorth et al. 2005; Berger et al. 2005). Recent observations suggest that short bursts reside at cosmological distances, while previous investigations showed that the spatial population of short GRBs seems to accord with lower redshift sources (e.g., Che et al. 1997; Magliocchetti et al. 2003; Tanvir et al. 2005). Therefore, the present research does not include redshift indictor of short bursts which is still at the prenatal stage.

Acknowledgements We would like to thank the anonymous referee for many helpful comments. It is our honor to thank D. Kocevski for useful suggestions in the preparation of this manuscript. This work was supported by the Special Funds for Major State Basic Research Projects (973) and the National Natural Science Foundation of China (Nos. 10273019 and 10463001).

References

Amati L., Frontera F., Tavani M. et al., 2002, A&A, 390, 81
Atteia J. L., 2003, A&A, 407, L1
Atteia J. L., 2005, astro-ph/0505074
Band D. L., 1997, ApJ, 486, 928
Berger E., Price P. A., CenkoBerger S. B. et al., 2005, Nature, 438, 988
Bloom J. S., Prochaska J. X., Pooley D. et al., 2006, ApJ, 638, 354
Bonnell J. T., Norris J. P., Nemiroff R. J. et al., 1997, ApJ, 490, 79
Che H., Yang Y., Wu M. et al., 1997, ApJ, 483, L25
Chen L., Lou Y.-Q., Wu M. et al., 2005, ApJ, 619, 983
Daigne F., Mochkovitch R., 2003, MNRAS, 342, 587
Dermer C. D., Mitman K. E., 1999, ApJ, 513, L5
Dermer C. D., Böttcher M., Chiang J., 1999, ApJ, 515, L49
Dermer C. D., Mitman K. E., 2004, ASPC, 312, 301
Eichler D., Levinson A., 2000, ApJ, 529, 146

Fenimore E. E., Epstein R. I., Ho C. et al., 1993, Nature, 366, 40
Galama T. J., Vreeswijk P. M., Rol E. et al., 1999, GCN, 388
Ghirlanda G., Ghisellini G., Celotti A., 2004a, A&A, 422, L55
Ghirlanda G., Ghisellini G., Lazzati D., 2004b, ApJ, 616, 331
Guidorzi C., Frontera F., Montanari E. et al., 2005, MNRAS, 363, 315
Gupta V., Gupta P. D., Bhat P. N., 2002, astro-ph/0206402
Hakkila J., Giblin T. W., 2004, ApJ, 610, 361
Hjorth J., Watson D., Fynbo J. et al., 2005, Nature, 437, 859
Hurley K., Kargatis V., Liang E. et al., 1992, AIPC, 265, 195
Hurley K. J., McBreen B., Quilligan F. et al., 1998, AIPC, 428, 191
Katz J., 1994, ApJ, 422, 248
Kobayashi S., Piran T., Sari R. 1997, ApJ, 490, 92
Kouveliotou C., Meegan C. A., Fishman G. J. et al., 1993, ApJ, 413, L101
Kocevski D., Ryde F., Liang E., 2003, ApJ, 596, 389
Kocevski D., Liang E., 2003, ApJ, 594, 385
Lee A., Bloom E. D., Petrosian V., 2000, ApJS, 131, 1
Li T. P., Qu J. L., Feng H. et al., 2004, ChJAA, 4, 583
Liang E. W., Xie G. Z., Su C. Y., 2002, PASJ, 54, 1
Lithwick Y., Sari R., 2001, ApJ, 555, 540
Magliocchetti M., Ghirlanda G., Celotti A., 2003, MNRAS, 343, 255
Mészáros P., Rees M. J., 1993, ApJ, 405, 278
McMahon E., Kumar P., Panaitescu A., 2004, MNRAS, 354, 915
McBreen B., Hurley K. J., Long R., Metcalfe L., 1994, MNRAS, 271, 662
McBreen S., Quilligan F., McBreen B. et al., 2001, A&A, 380, L31
McBreen S., Quilligan F., McBreen B. et al., 2003, AIPC, 662, 280
Nakar E., Piran T., 2002, MNRAS, 330, 920
Norris J. P., Nemiroff R. J., Bonnell J. T. et al., 1996, ApJ, 459, 393
Norris J. P., Marani G. F., Bonnell J. T., 2000, ApJ, 534, 248
Norris J. P., Scargle J. D., Bonnell J. T., 2001, astro-ph/0105108
Norris J. P., Bonnell J. T., Kazanas D. et al., 2004, A&AS, 205, 6804
Norris J. P., Bonnell J. T., Kazanas D. et al., 2005, ApJ, 627, 324
Piran T., Shemi A., Narayan R., 1993, MNRAS, 263, 861
Piran T., 1999, Physics Reports, 314, 575
Press W. H., Teukolsky S. A., Vetterling W. T. et al., 1992, Numerical Recipies in FORTRAN, Cambridage: Cambridage Univ. Press, p.640
Qin Y. P., Zhang Z. B., Zhang F. W. et al., 2004, ApJ, 617, 439
Qin Y. P., Dong Y. M., Lu R. J. et al., 2005, ApJ, 632, 1008
Quilligan F., McBreen B., Hanlon L. et al., 2002, A&A, 385, 377
Reichart D. E., Lamb D. Q., Fenimore E. E. et al., 2001, ApJ, 552, 57
Rees M. J., Mészáros P., 1994, ApJ, 430, L93
Ryde F., Borgonovo L., Larsson S. et al., 2003, A&A, 411, L331
Ryde F., Kocevski D., Bagoly Z. et al., 2005, A&A, 432, 105
Sari R., Piran T., 1996, AIPC, 384, 782
Sari R., Piran T., 1997, ApJ, 485, 270
Scargle J. D., 1998, ApJ, 504, 405
Schaefer B. E., Deng M., Band D. L., 2001, ApJ, 563, L123
Schaefer B. E., 2004, ApJ, 602, 306
Shen R. F., Song L. M., Li Z., 2005, MNRAS, 362, 59
Spada M., Panaitescu A., Mészáros P., 2000, ApJ, 537, 824
Tanvir N. R., Chapman R., Levanet A. J. et al., 2005, Nature, 438, 991
Woods E., Loeb A., 1995, ApJ, 453, 583
Yonetoku D., Murakami T., Nakamura T. et al., 2004, ApJ, 609, 935
Zhang Z. B., Qin Y. P., 2005, MNRAS, 363, 1290